

1
2
3
4
5
6
7
8
9
10
11
12
13
14
15
16
17
18
19

Supplementary information for:

**GTWS-MLrec: Global terrestrial water storage reconstruction by
machine learning from 1940 to present**

Jiabo Yin¹, Louise J. Slater², Abdou Khouakhi³, Le Yu^{4,5,6}, Pan Liu¹, Fupeng Li⁷, Yadu Pokhrel⁸, Pierre Gentine^{9,10}

¹State Key Laboratory of Water Resources Engineering and Management, Wuhan University, Wuhan, Hubei, 430072, P.R. China

²School of Geography and the Environment, University of Oxford, Oxford, UK

³School of Water, Energy and Environment, Cranfield Environment Centre, Cranfield University, UK

⁴Department of Earth System Science, Ministry of Education Key Laboratory for Earth System Modeling, Institute for Global Change Studies, Tsinghua University, Beijing, China

⁵Ministry of Education Ecological Field Station for East Asian Migratory Birds, Beijing, China

⁶Tsinghua University (Department of Earth System Science)- Xi'an Institute of Surveying and Mapping Joint Research Center for Next-Generation Smart Mapping, Beijing, China

⁷Institute of Geodesy and Geoinformation, University of Bonn, Bonn, Germany

⁸Department of Civil and Environmental Engineering, Michigan State University, East Lansing, MI, USA

⁹Department of Earth and Environmental Engineering, Columbia University, New York, NY, USA

¹⁰Climate School, Columbia University, New York, NY, USA

20 **Text S1: Skill metrics computation**

21 Eight skill metrics are used to evaluate model performance: Pearson's Correlation
22 Coefficient (PCC), Nash-Sutcliffe efficiency coefficient (NSE); Kling-Gupta
23 Efficiency coefficient (KGE), Coefficient of Determination (R^2), Root Mean square
24 error (RMSE); normalized Root Mean Square Error (nRMSE), Mean Absolute
25 Percentage Error (MAPE), and Percent bias (Pbias, unit: %).

26 PCC measures the linear correlation between modeled and observed TWS
27 anomalies, and is expressed as:

$$28 \quad \text{PCC} = \frac{\text{COV}(Q_m, Q_o)}{\sigma_{Q_m} \sigma_{Q_o}} \quad (1)$$

29 where Q_m and Q_o are the reconstructed and observed TWS anomalies respectively; COV
30 is the covariance of Q_m and Q_o ; σ_{Q_m} and σ_{Q_o} are the standard deviations of the modeled
31 and observed TWS anomalies, respectively.

32 The NSE metric is widely used to determine overall model efficiency in
33 hydrological fields, and is computed from model-simulated and observed TWS
34 anomalies time series as follows:

$$35 \quad \text{NSE} = 1 - \frac{\sum_{t=1}^T (Q_m^t - Q_o^t)^2}{\sum_{t=1}^T (Q_o^t - \overline{Q_o})^2} \quad (2)$$

36 where Q_m^t and Q_o^t are modeled and observed TWS anomalies at time t . $\overline{Q_o}$ is the
37 mean observed TWS anomalies. NSE can range from $-\infty$ to 1, and the closer the NSE
38 is to 1, the more reliable is the match between modeled and inferred TWS anomalies
39 time series.

40 KGE measures the Euclidean distance between a point and the optimal point, and
41 is calculated as:

42
$$KGE = 1 - \sqrt{(PCC - 1)^2 + (BR - 1)^2 + (RV - 1)^2}$$
 (3)

43 where

44
$$BR = \overline{Q_m}/\overline{Q_o}$$
 (4)

45 and

46
$$RV = (\sigma Q_m/\overline{Q_m})/(\sigma Q_o/\overline{Q_o})$$
 (5)

47 A KGE of 1 indicates perfect agreement between simulations and simulated TWS
 48 anomalies.

49 R^2 measures the proportion of variation in the dependent variable explained by the
 50 predictors included in the model, which is expressed as:

51
$$R^2 = 1 - \left(\frac{\sum_{t=1}^T (Q_m^t - Q_o^t)^2}{\sum_{t=1}^T (Q_o^t - \overline{Q_o})^2} \right)$$
 (6)

52 When the R^2 is approaching 1, it means that the model has better performance.

53 The RMSE is a frequently used measure of the differences between predictors and
 54 the observations:

55
$$RMSE = \sqrt{\frac{\sum_{t=1}^T (Q_m^t - Q_o^t)^2}{T}}$$
 (7)

56 RMSE can be used to compare different models. However, RMSE does not
 57 perform well if comparing models fits for different response variables or if the response
 58 variable is standardized, log-transformed, or otherwise modified. To overcome these
 59 issues, the NRMSE is also used:

60
$$nRMSE = \frac{RMSE}{\sigma Q_o} = \frac{\sqrt{\sum_{t=1}^T (Q_m^t - Q_o^t)^2}}{\sqrt{\sum_{t=1}^T (Q_o^t - \overline{Q_o})^2}}$$
 (8)

61

62 The MAPE measures the accuracy of model forecasts as a percentage. It can be
63 calculated as the average of the absolute differences between predicted and actual
64 values, divided by the actual values, for each time period.

$$65 \quad MAPE = \frac{1}{T} \sum_{t=1}^T \left| \frac{Q_m^t - Q_0^t}{Q_0^t} \right| \quad (9)$$

66 Pbias measures the percentage bias of modeled TWS anomalies that are larger or
67 smaller than the corresponding inferred natural TWS anomalies. A Pbias of 0 indicates
68 perfect alignment. Pbias is computed as:

$$69 \quad Pbias = \frac{\sum_{t=1}^T (Q_m^t - Q_0^t)}{\sum_{t=1}^T Q_0^t} \times 100\% \quad (10)$$

70 For the metrics of RMSE, nRMSE, MAPE and Pbias, a smaller metric value
71 indicates better performance of the model simulations.

72

73

74

75

76

77

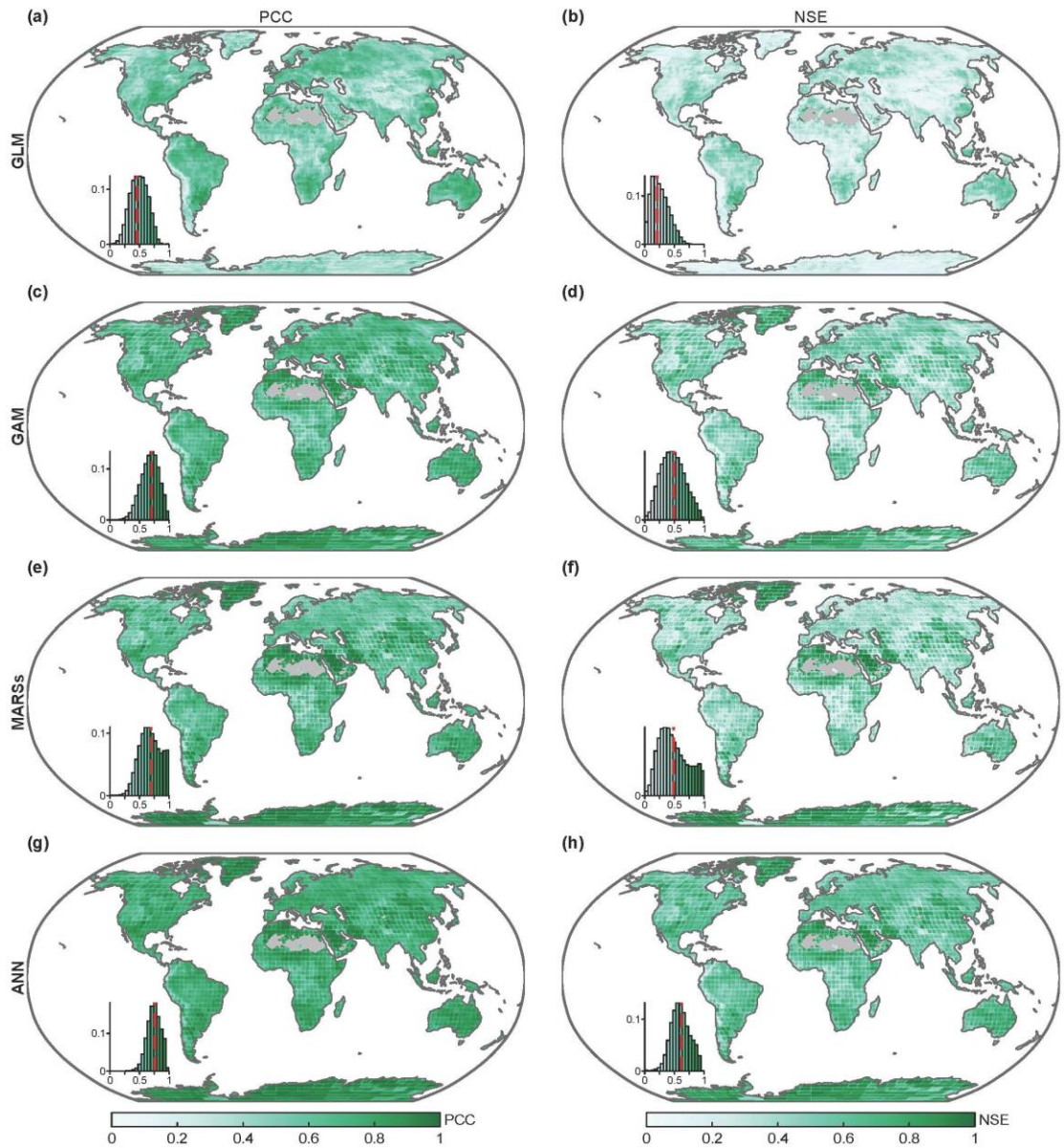
78

79

80

81

82



83

84 **Figure S1.** Performance of different machine learning models in simulating JPL TWS anomalies under

85 scheme 8 during the test period. The left plots indicate the value of PCC, and the right plots show the

86 value of NSE. Insets in each figure show the histogram of these metrics, with the dashed vertical line

87 showing the median value. Data-sparse areas without reconstruction are marked in grey.

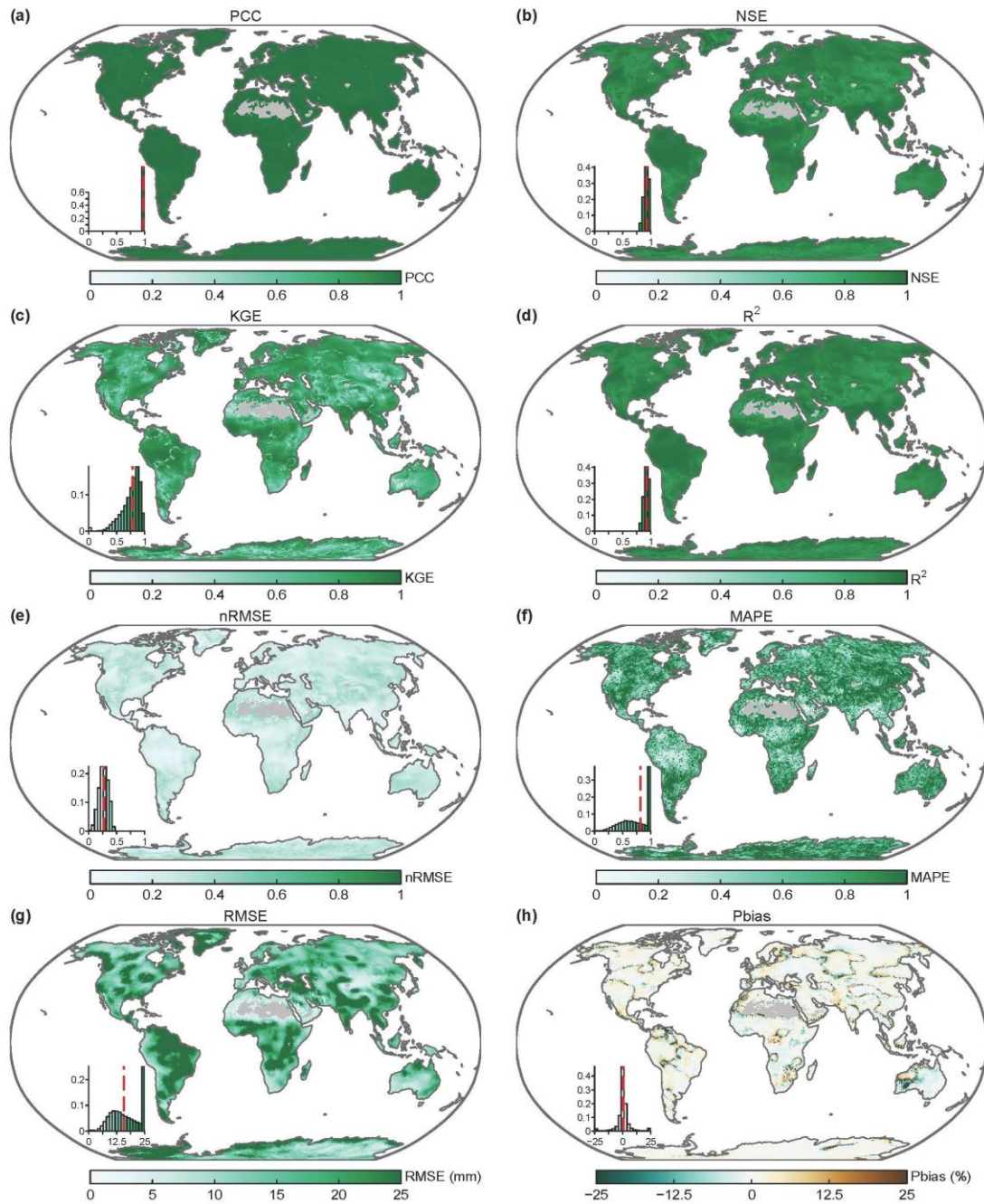
88

89

90

91

92



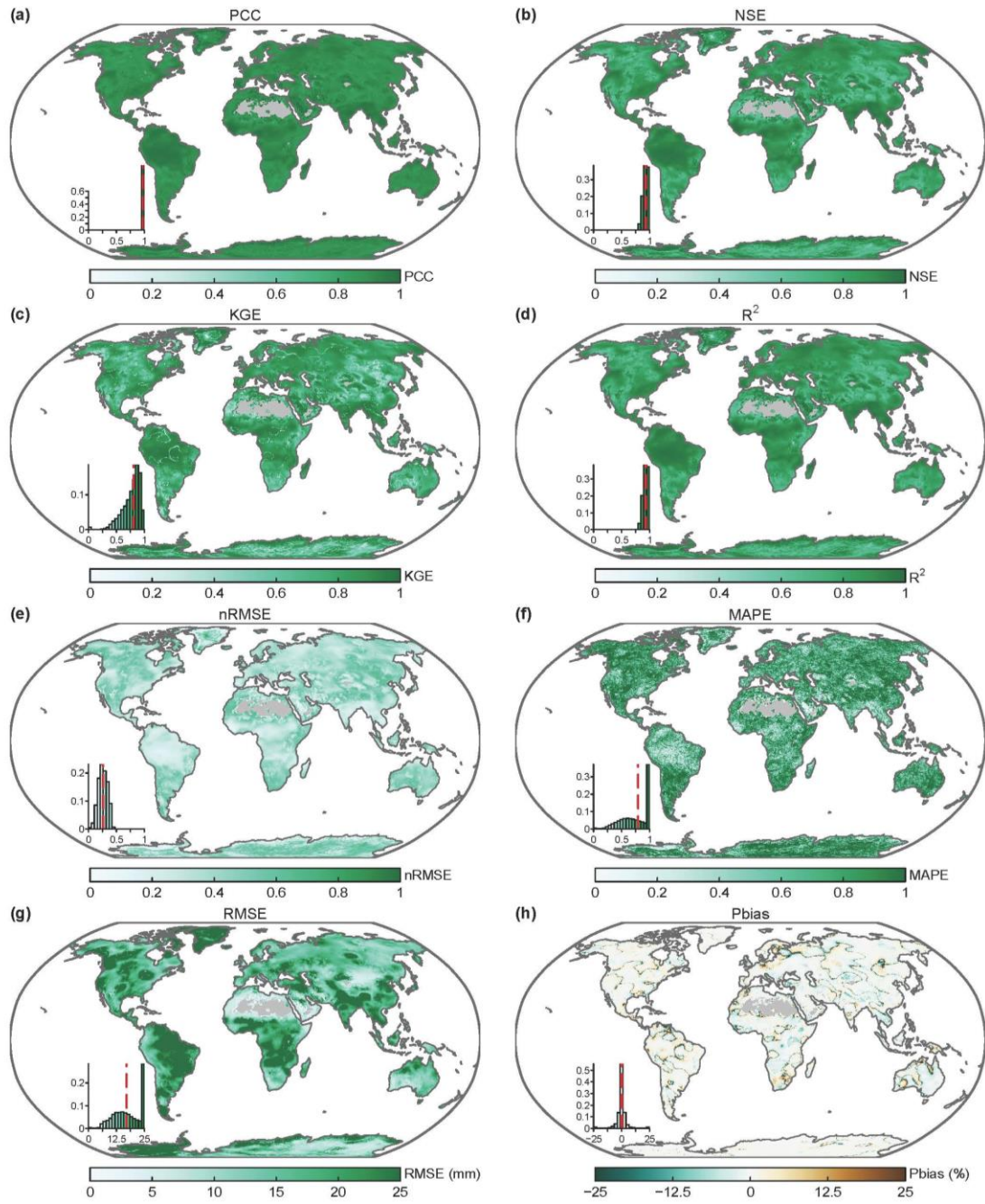
93

94 **Figure S2.** Comparison of our reconstructed CSR TWS anomalies against the GRACE/GRACE-FO
 95 observations. Insets in each figure show the histogram of these metrics, with the dashed vertical line
 96 showing the median value. Data-sparse areas without reconstruction are marked in grey.

97

98

99



100

101

Figure S3. Comparison of our reconstructed GSFC TWS anomalies against the GRACE/GRACE-FO

102

observations. Insets in each figure show the histogram of these metrics, with the dashed vertical line

103

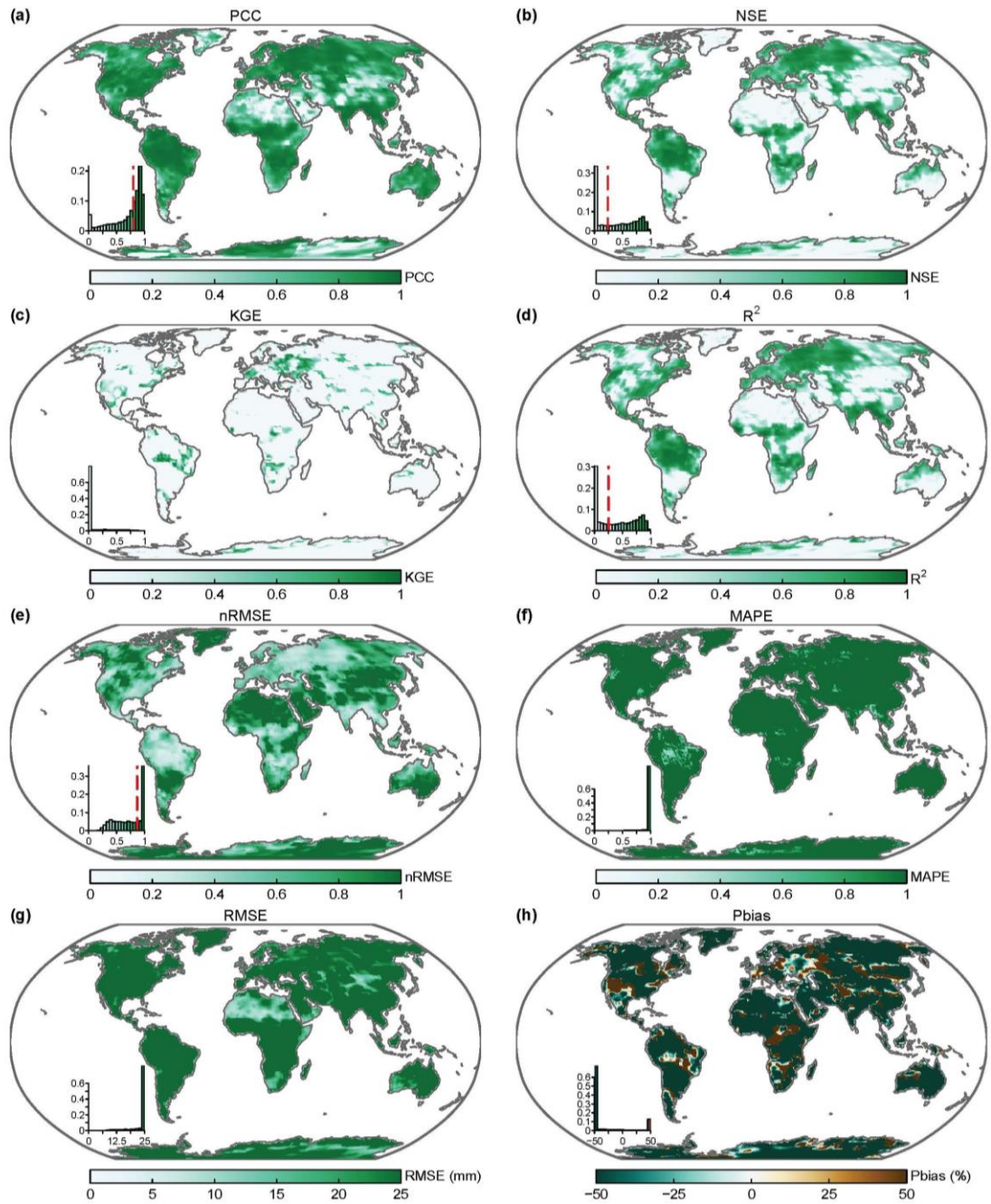
showing the median value. Data-sparse areas without reconstruction are marked in grey.

104

105

106

107



108

109

Figure S4. Comparison of the GRACE-REC dataset against the GRACE/GRACE-FO observations.

110

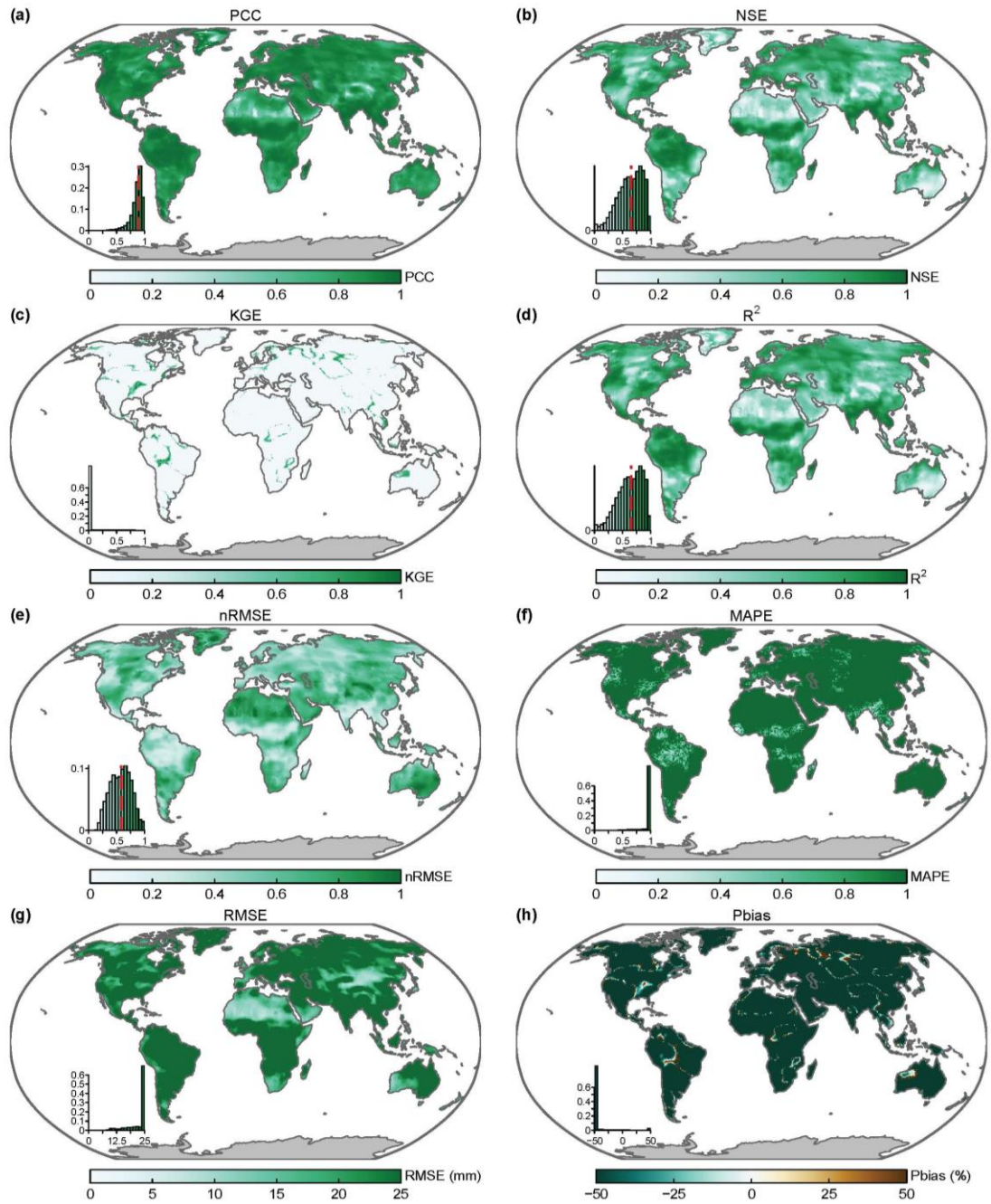
Insets in each figure show the histogram of these metrics, with the dashed vertical line showing the

111

median value. Data-dense areas without reconstruction are marked in grey.

112

113



114

115

Figure S5. Comparison of the GRL reconstructed dataset against the GRACE/GRACE-FO observations.

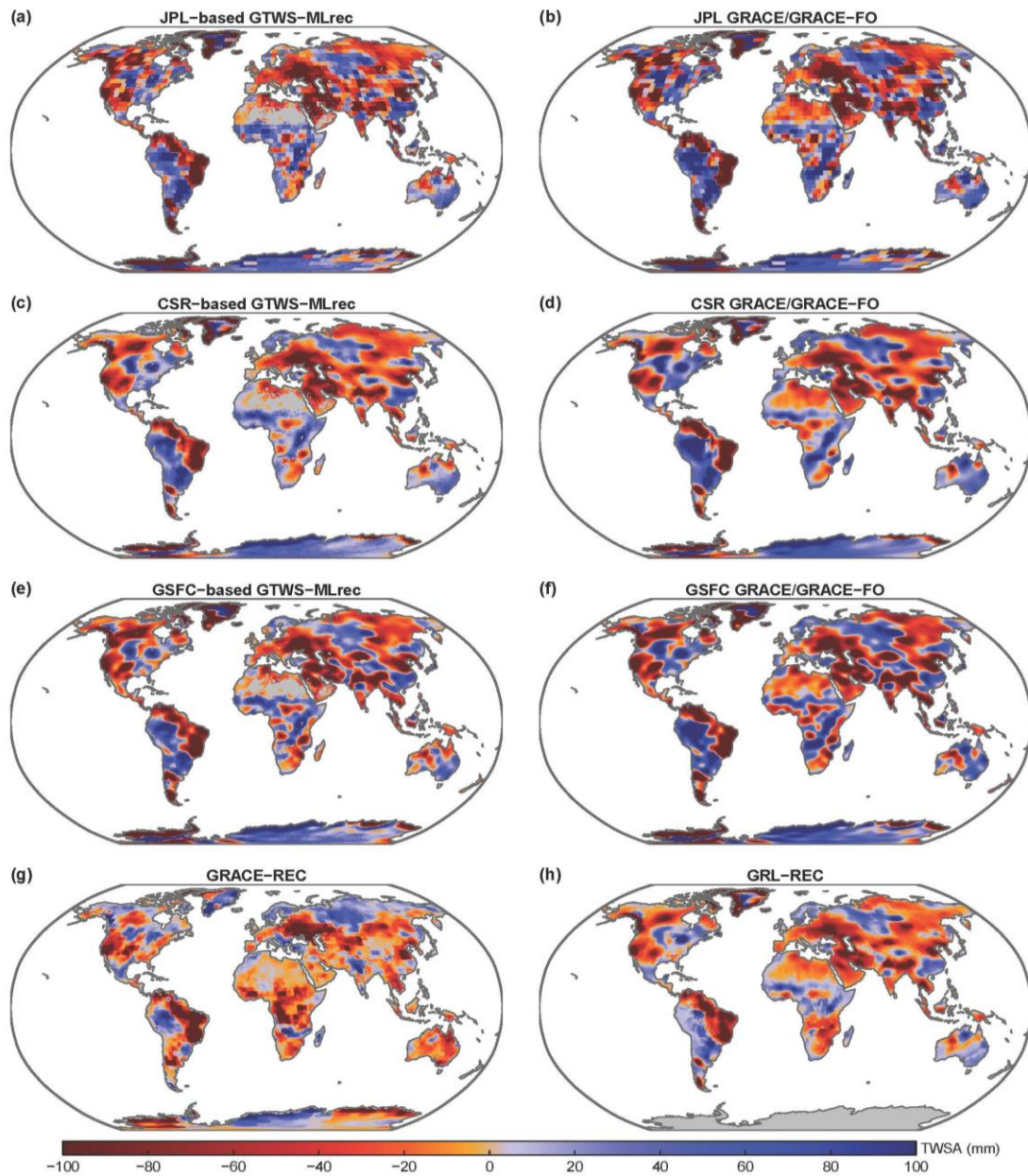
116

Insets in each figure show the histogram of these metrics, with the dashed vertical line showing the

117

median value. Data-dense areas without reconstruction are marked in grey.

118

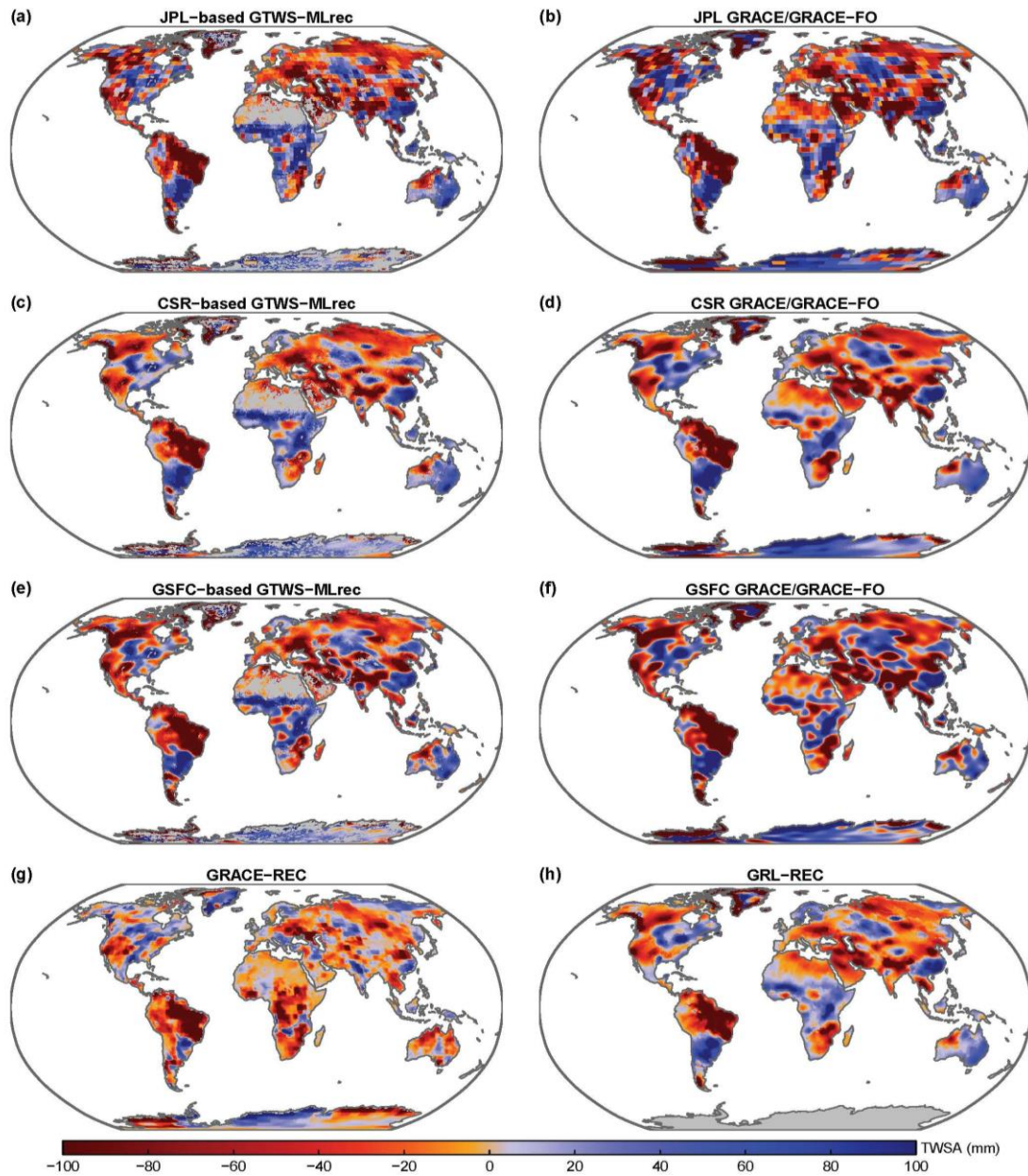


119

120 **Figure S6.** Global map of TWS anomalies in 2015 under GRACE/GRACE-FO (right column) and for

121 the different reconstruction datasets (left column).

122

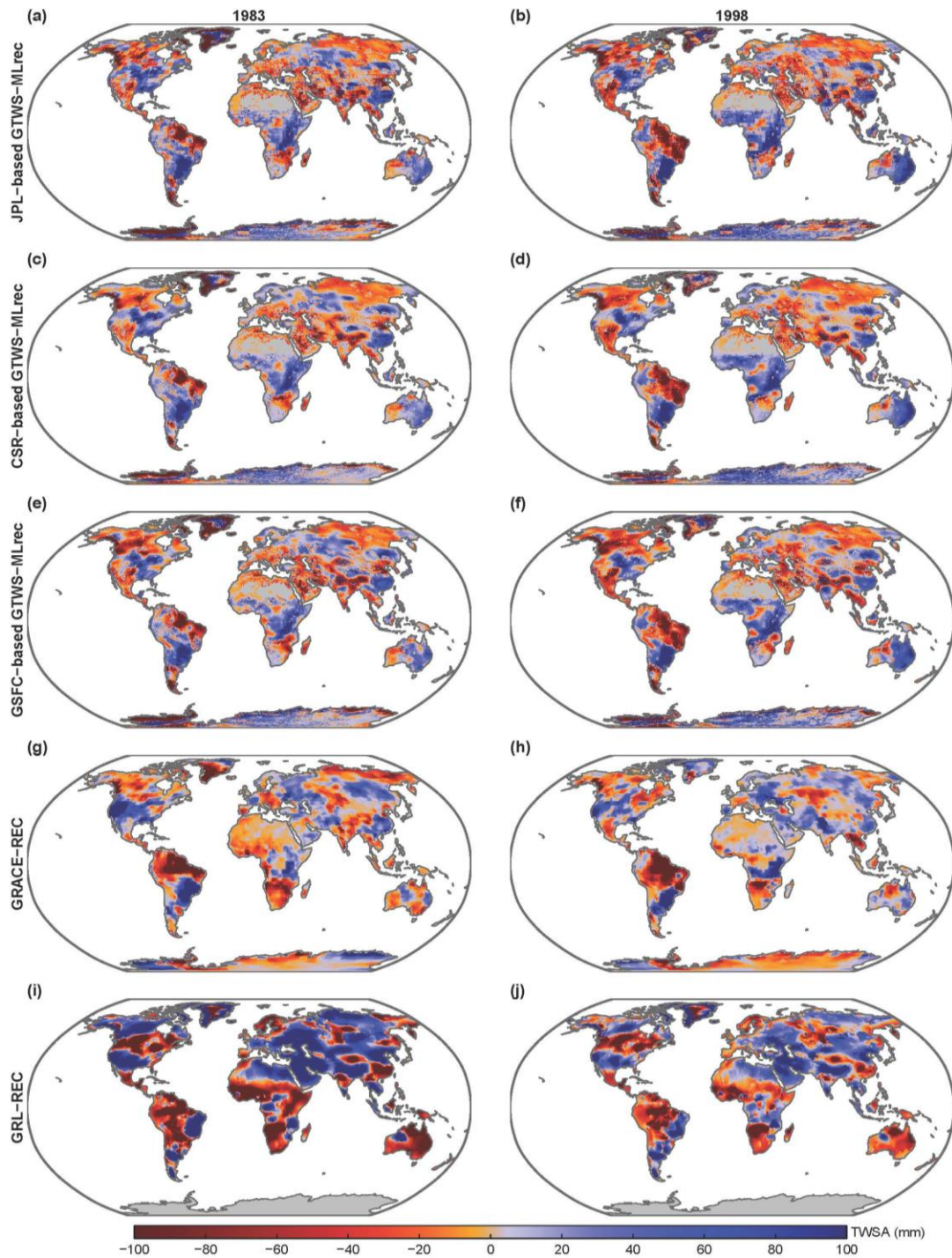


123

124 **Figure S7.** Global map of TWS anomalies in 2016 under GRACE/GRACE-FO and for the different

125 reconstruction datasets.

126



127

128 **Figure S8.** Global map of TWS anomalies in 1983 (left column) and 1998 (right column) for the different

129 reconstruction datasets.